

Thermal conduction force under standing and quasistanding temperature field

Haohan Tan, Yuqian Zhao, and Jiping Huang *

Department of Physics, State Key Laboratory of Surface Physics, and Key Laboratory of Micro and Nano Photonic Structures (MOE), Fudan University, Shanghai 200438, China

 (Received 7 January 2024; accepted 21 March 2024; published 9 April 2024)

Thermal conduction force plays a crucial role in manipulating the local thermal conductivity of crystals. However, due to the diffusive nature of thermal conduction, investigating the force effect is challenging. Recently, researchers have explored the force effect based on the wavelike behavior of thermal conduction, specifically second sound. However, their focus has been primarily on the progressive case, neglecting the more complex standing temperature field case. Additionally, establishing a connection between the results obtained from the progressive case and the standing case poses a challenging problem. In this study, we investigate the force effect of standing and quasistanding temperature fields, revealing distinct characteristics of thermal conduction force. Moreover, we establish a link between the progressive and standing cases through the quasistanding case. Our findings pave the way for research in more intricate scenarios and provide an additional degree of freedom for manipulating the local thermal conductivity of dielectric crystals.

DOI: [10.1103/PhysRevE.109.044124](https://doi.org/10.1103/PhysRevE.109.044124)

I. INTRODUCTION

Thermal conduction is a research field that has garnered significant attention, both from a macroscopic and microscopic perspective [1–12]. However, the force effect associated with this heat transport mechanism has received limited attention. In this regard, the thermal conduction force between the liquid-liquid and liquid-solid phases has been theoretically explained and experimentally verified by considering the coupling of momentum and flux [13–15]. For the solid-solid case, Tan *et al.* proposed the theory of second sound radiation force (SSRF) based on the wavelike nature of thermal conduction in dielectric crystals [16–22]. Their work not only confirmed the existence of SSRF but also demonstrated its tunability by manipulating the incident wave. This research challenges the conventional notion that a constant temperature gradient is necessary to induce thermal conduction force. Moreover, SSRF provides a mechanism for manipulating local thermal conductivity [23,24].

However, Tan *et al.* only investigated the case of a single incident second sound [16]. To further advance the research, it is necessary to explore the scenario involving multiple incident second sounds. When two second sounds with equal amplitudes counter-propagate, they create a standing temperature field, while different amplitudes result in a quasistanding temperature field. Consequently, the thermal conduction force becomes more complex. First, it is unknown whether the force exhibits distinct behavior compared to the progressive case under these two scenarios. Second, it remains uncertain whether changing the force direction, as previously observed, holds the same significance. Furthermore, we are particularly interested in determining if there is a

relationship between the results obtained from these different cases. In this study, we theoretically investigate the thermal conduction force exerted on stationary and adiabatic impurity particles in dielectric crystals when two counter-propagating second sounds generate standing and quasistanding temperature fields. We consider various cases, including the plane, zeroth-order Bessel, and high-order Bessel standing cases. Additionally, we examine the corresponding quasistanding cases. Interestingly, we discover that the force direction can be reversed, similar to the progressive case. However, due to the absence of a specific propagating direction for the standing and quasistanding temperature fields, their physical implications differ. The most significant finding is that the results obtained from the quasistanding case establish a connection between the results of the standing and progressive cases. These findings not only enhance the theoretical understanding of thermal conduction force but also provide an additional degree of freedom for manipulating the local thermal conductivity of dielectric crystals, as is shown in Fig. 1(c).

II. GENERAL THEORY FOR CALCULATING THERMAL CONDUCTION FORCE

To investigate the standing and quasistanding temperature field's impact on the SSRF, we utilize the nonattenuation model as a progressive case. Initially, we assume that the dielectric crystal's temperature is approximately 10 K, ensuring that phonon transport operates within the hydrodynamic regime. In certain crystalline materials, the phenomenon of second sound is observed at a temperature of 10 K [20]. Subsequently, we assume that the resistive process can be neglected, implying an infinite resistive relaxation time, $\tau_R \rightarrow \infty$. Additionally, we consider the normal relaxation time τ_N to be sufficiently short. Consequently, we can assume that the phonon system can be described by the local equilibrium

*jphuang@fudan.edu.cn

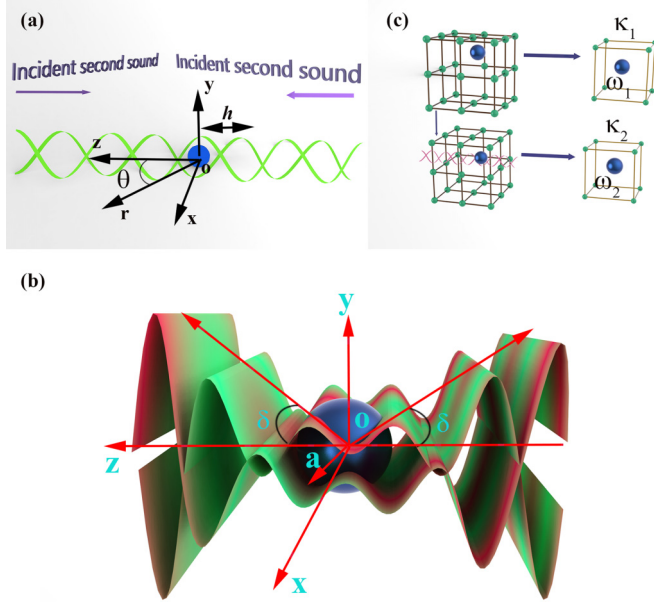


FIG. 1. Schematic of thermal conduction force under standing and quasistanding temperature field. (a) An adiabatic spherical particle in the presence of plane standing temperature field is depicted. The particle center is the origin of the Cartesian coordinate system (x, y, z) , and θ denotes the polar angle. (b) A particle with radius a in the presence of Bessel standing second sound is shown, with δ representing the half cone angle. (c) The local thermal conductivity of dielectric crystals can be tuned by manipulating the interaction between the impurity particle (the blue sphere) and the second sound (the pink wave). ω_1 and ω_2 are the vibrating angular frequencies of the impurity particle before and after interacting with the second sound, and κ_1 and κ_2 are the corresponding local thermal conductivities of the crystal. The region containing the impurity particle is zoomed in for clarity.

function

$$f(\mathbf{k}, \mathbf{r}, t) = \frac{1}{e^{\beta(\mathbf{r}, t)(\hbar\omega_{\mathbf{k}} - \hbar\mathbf{k}\cdot\mathbf{u}(\mathbf{r}, t))} - 1}, \quad (1)$$

where \hbar , $\omega_{\mathbf{k}}$, \mathbf{k} , and $\mathbf{u}(\mathbf{r}, t)$ are the reduced Planck constant, phonon angular frequency, phonon wave vector, and phonon drifting velocity, respectively. $\beta(\mathbf{r}, t) = 1/(k_B T(\mathbf{r}, t))$, where k_B is the Boltzmann constant, and $T(\mathbf{r}, t)$ is the local temperature of the crystal. \mathbf{r} is the position vector, and t represents time. In the aforementioned premises, the second and third assumptions rest upon the fact that in any crystal, both resistive and normal processes occur. When the normal process predominates in phonon collisions, the impact of the resistive process can be considered negligible, signified by $\tau_R \rightarrow \infty$. Consequently, it is justifiable to treat the phonon system as being in a state of local equilibrium. In our investigation of the force effect of second sound, the size of the impurity particle has an impact on the resistive relaxation time. However, our focus lies within the regime where $\tau_N \ll \tau_R$. Under this condition, the local equilibrium assumption remains valid, even as the radius of the impurity particle, denoted as a , varies. Through the application of momentum and energy conservation principles, as well as the utilization of the Debye model to characterize the phonon spectrum, we are able to provide

evidence supporting the propagation of the temperature field as a wave phenomenon known as second sound [25–32].

According to the momentum conservation law, we can define the SSRF as the progressive case,

$$F = - \iint \langle \Pi' \rangle dS, \quad (2)$$

where $\Pi'_{ij} = \sum_{\mathbf{k}} \hbar k_i v_{k_j} (f - f_0)$ is the momentum flux of the second sound, and $v_{k_j} = \partial\omega_{\mathbf{k}}/\partial k_j$ is the phonon group velocity component. The variable F denotes the time-averaged force exerted on a particle by the temperature field. The integration is over the particle surface S . In this context, the term $f - f_0$ represents the deviation of the phonon system from its equilibrium state, which is characterized by f_0 . The equilibrium state of the system is given by the equation

$$f_0(\mathbf{k}) = \frac{1}{e^{\beta_0 \hbar \omega_{\mathbf{k}}} - 1}, \quad (3)$$

where $\beta_0 = 1/k_B T_0$, and T_0 represents the background temperature. In the equilibrium state ($f = f_0$), there is no SSRF present.

For the sake of simplicity, we assume that one incident second sound propagates along the $+z$ direction, while the other propagates along the $-z$ direction. Under this assumption, Eq. (2) can be further simplified as follows:

$$F = - \iint \sum_{\mathbf{k}} \hbar k_z v_{k_z} (f - f_0) dS. \quad (4)$$

After further derivation, we can obtain the expression for the SSRF under the standing and quasistanding case:

$$F = -\frac{1}{2} \times \iint \left(\frac{2\pi^2}{9\beta_0^4 (\hbar c)^3} \left\langle \left(\frac{T'_1}{T_0} \right)^2 \right\rangle + \frac{\pi^2}{15\beta_0^4 \hbar^3 c^5} \langle |u|^2 \rangle \right) dS. \quad (5)$$

Here, c represents the modulus of the phonon group velocity. It is noteworthy that the expression derived above for the SSRF is identical to the one obtained in the progressive case. However, in this context, T'_1 represents the sum of two incident second sounds and their corresponding scattering field. When calculating the acoustic radiation force in the acoustic field, two methods are commonly employed: the angular-spectrum method and the multipole-expansion based method. Extensive research has demonstrated the equivalence of these two approaches [33–40]. In the subsequent analysis, we will utilize the multipole-expansion based method for direct calculations.

III. FORCE EFFECTS WITH DIFFERENT STANDING AND QUASI-STANDING TEMPERATURE FIELDS

Initially, we examine the SSRF under a plane standing temperature field. In this scenario, the incident second sound can be mathematically represented as $T_{\text{inc}} = T_1 e^{-i\omega t} \{e^{iq(z+h)} + e^{-iq(z+h)}\}$, where T_1 , ω , and q denote the amplitude, angular frequency, and wave number of the second sound, respectively. Here, h represents the distance in the z direction from the center of the impurity to the nearest velocity antinode, as

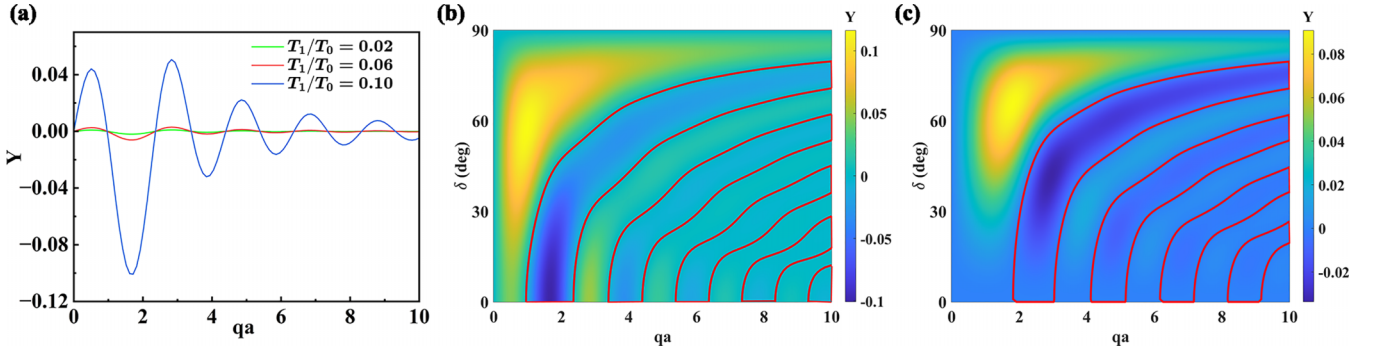


FIG. 2. Numerical results of the reduced second sound radiation force Y_{st} under the conditions of (a) plane standing second sound as a function of qa (where q and a are the second sound wave number and the particle radius) with the temperature ratio $T_1/T_0 = 0.02, 0.06, 0.10$ (where T_1 is the second sound amplitude, and T_0 is the background temperature), (b) zeroth-order Bessel standing second sound as a function of qa and δ (unit: degree) with $T_1/T_0 = 0.10$, and (c) first-order Bessel standing second sound as a function of qa and δ with $T_1/T_0 = 0.10$. The area enclosed by the red line is where $Y_{st} < 0$.

is shown in Fig. 1(a). Additionally, $i = \sqrt{-1}$, and t signifies time. By expressing the incident second sound in spherical coordinates, we can derive the following expression:

$$T_{\text{inc}} = T_1 \sum_{n=0}^{\infty} (2n+1) \Lambda_n i^n j_n(qr) P_n(\cos \theta) e^{-i\omega t}, \quad (6)$$

where $j_n(x)$ is the spherical Bessel function of order n , $P_n(x)$ are the Legendre polynomial of order n , $\Lambda_n = \{e^{iq(z+h)} + e^{-iq(z+h)}\}$, and θ is the polar angle. Following the calculation procedure in progressive case, we can get the SSFR for the plane standing second sound:

$$F = -\frac{2\pi^3 a^2 T_1^2}{9\beta_0^4 (\hbar c)^3 T_0^2} \sum_{n=0}^{\infty} 4(-1)^{n+1} n(n+1)(n+2) \times [U_n(qa)U_{n+1}(qa) + V_n(qa)V_{n+1}(qa)] \sin(2qh) - \frac{\pi^3 T_1^2}{5\beta_0^4 (\hbar c)^3 q^2 T_0^2} \sum_{n=0}^{\infty} 4(-1)^{n+1} (n+1) \times [U_n(qa)U_{n+1}(qa) + V_n(qa)V_{n+1}(qa)] \sin(2qh), \quad (7)$$

where U and V are determined by the scattering characteristics of the second sound at the boundary of the impurity particle. As we are examining the force effect on a stationary and adiabatic impurity particle, the expressions for U and V remain the same as in the progressive case:

$$U_n(qa) = j_n(qa) - \frac{j_n(qa)}{j_n'^2(qa) + g_n'^2(qa)} \times [j_n'(qa)j_n(qa) + g_n'(qa)g_n(qa)], \quad (8)$$

$$V_n(qa) = \frac{j_n(qa)}{j_n'^2(qa) + n_n'^2(qa)} \times [j_n(qa)g_n'(qa) - j_n'(qa)g_n(qa)], \quad (9)$$

where $g_n(x)$ is the spherical Bessel function of order n of the second kind, and $j_n'(x)$ and $g_n'(x)$ are the derivatives of $j_n(x)$ and $g_n(x)$ with respect to x , respectively. Consequently, the reduced SSFR, i.e., the time-averaged force exerted on the particle per unit energy density and per scattering cross

section, can be expressed as follows:

$$Y_{st} = \frac{F}{AE_1' \sin(2qh)} = \frac{F}{\pi a^2 E_1' \sin(2qh)} = -\frac{5T_1}{3T_0} \sum_{n=0}^{\infty} 4(-1)^{n+1} n(n+1)(n+2) \times [U_n(qa)U_{n+1}(qa) + V_n(qa)V_{n+1}(qa)] - \frac{3T_1}{2T_0(qa)^2} \sum_{n=0}^{\infty} 4(-1)^{n+1} (n+1) \times [U_n(qa)U_{n+1}(qa) + V_n(qa)V_{n+1}(qa)], \quad (10)$$

where A represents the cross-section area, and E' denotes the characteristic energy density of the incident second sound [16]. The results of Y_{st} for different values of T_1/T_0 are illustrated in Fig. 2(a). Unlike the progressive case [41–47], where only positive Y_p values are observed, here, even in the case of the plane standing second sound, negative Y_{st} values can be obtained. In the context of the standing second sound, where there is no specific propagation direction, a negative Y_{st} value indicates that the direction of SSRF is toward the temperature antinode. Conversely, a positive Y_{st} value signifies that the force direction is toward the temperature node. This stands in contrast to the progressive case. It is worth noting that, in the presence of a plane standing sound wave field, the reduced SSRF can exhibit both positive and negative values [48], further supporting the validity of our findings.

Next, when the incident field is a standing zeroth-order Bessel second sound, the temperature field can be expressed as $T_{\text{inc}} = T_1 e^{-i\omega t} \{e^{iq_z(z+h)} + e^{-iq_z(z+h)}\} J_0(q_r \sin \theta)$. Here, q_z and q_r represent the axial and radial wave numbers, respectively, i.e., $q = \sqrt{q_z^2 + q_r^2}$. $J_0(x)$ denotes the cylindrical Bessel function of zeroth order. Similarly, in spherical coordinates, the incident field can also be expressed as Eq. (6). But the expression of Λ_n is different. Here, $\Lambda_n = \{e^{iq_z(z+h)} + e^{-iq_z(z+h)}\} P_n(\cos \delta)$, $\delta = \cos^{-1}(q_z/q)$ is the half cone angle of the incident second sound [see Fig. 1(b)]. It is easy to verify

that

$$\begin{aligned}
Y_{st} = & -\frac{5T_1}{3T_0} \sum_{n=0}^{\infty} 4(-1)^{n+1}(n+1)[U_n(qa)U_{n+1}(qa) \\
& + V_n(qa)V_{n+1}(qa)]P_n \cos(\delta)P_{n+1} \cos(\delta) \\
& -\frac{3T_1}{2T_0(qa)^2} \sum_{n=0}^{\infty} 4(-1)^{n+1}n(n+1)(n+2)[U_n(qa) \\
& \times U_{n+1}(qa) + V_n(qa)V_{n+1}(qa)]P_n \cos(\delta)P_{n+1} \cos(\delta).
\end{aligned} \tag{11}$$

Here, the standing temperature field can be seen as the superposition of two progressive second sounds with the same half cone angle δ . The variation of Y_{st} with qa is shown in Fig. 2(b). In contrast to the progressive zeroth-order Bessel second sound, Y_{st} can be negative in this case, indicating the same behavior as in the plane standing case. Meanwhile, when $\delta = 0$, the result is equivalent to the plane standing case, as the zeroth-order Bessel second sound reduces to plane standing second sound. The comparison with the acoustic radiation force under a zeroth-order Bessel standing sound wave field confirms the reasonableness of our results [49]. Further, we investigate the SSRF for first-order Bessel standing second sound. The incident second sound can be mathematically represented as $T_{inc} = T_1 e^{-i\omega t} \{e^{iq_z(z+h)} + e^{-iq_z(z+h)}\} J_1(q_r \sin \theta) e^{i\phi}$, where $J_1(x)$ denotes the cylindrical Bessel function of the first order, and ϕ denotes the azimuth angle. By transforming this expression into spherical coordinates, we can derive the following results:

$$\begin{aligned}
T_{inc} = & T_1 \sum_{n=1}^{\infty} \frac{(n-1)!}{(n+1)!} (2n+1) \Lambda_n i^{n-1} j_n(qr) \\
& \times P_n^1(\cos \theta) e^{-i\omega t} e^{i\phi}.
\end{aligned} \tag{12}$$

Here, $\Lambda_n = \{e^{iq_z(z+h)} + (-1)^{n+1} e^{-iq_z(z+h)}\} P_n^1(\cos \delta)$, and $P_n^m(x)$ is the associated Legendre polynomial. Following the same procedure as before, the reduced SSRF is

$$\begin{aligned}
Y_{st} = & -\frac{5T_1}{3T_0} \sum_{n=1}^{\infty} \frac{4(-1)^{n+2}}{n+1} [U_n(qa)U_{n+1}(qa) \\
& + V_n(qa)V_{n+1}(qa)]P_n \cos(\delta)P_{n+1} \cos(\delta)
\end{aligned}$$

$$\begin{aligned}
& -\frac{3T_1}{2T_0(qa)^2} \sum_{n=1}^{\infty} \frac{4(-1)^{n+2}n(n+2)}{n+1} [U_n(qa)U_{n+1}(qa) \\
& + V_n(qa)V_{n+1}(qa)]P_n \cos(\delta)P_{n+1} \cos(\delta).
\end{aligned} \tag{13}$$

The results demonstrate that Y_{st} can exhibit both positive and negative values [see Fig. 2(c)]. This finding aligns with the acoustic radiation force observed under a one-order Bessel standing sound wave field, as reported by Mitri *et al.* [50].

As previously mentioned, the standing second sound can be conceptualized as the superposition of two second sounds propagating with the same amplitude. When these two second sounds possess different amplitudes, they give rise to a quasistanding temperature field. For instance, considering the case of a plane quasistanding field, the incident temperature field can be mathematically represented as $T_{inc} = e^{-i\omega t} \{T_1 e^{iq(z+h)} + T_2 e^{-iq(z+h)}\}$, where we assume $T_1 > T_2$. By employing the direct calculation method, we can determine the SSRF for the plane quasistanding temperature field:

$$\begin{aligned}
Y_{qst} = & -\left(\frac{T_2 \sin(2qh)}{T_1}\right) \frac{5T_1}{3T_0} \sum_{n=0}^{\infty} 4(-1)^{n+1}n(n+1)(n+2) \\
& \times [U_n(qa)U_{n+1}(qa) + V_n(qa)V_{n+1}(qa)] \\
& -\left(\frac{T_2 \sin(2qh)}{T_1}\right) \frac{3T_1}{2T_0(qa)^2} \sum_{n=0}^{\infty} 4(-1)^{n+1}(n+1) \\
& \times [U_n(qa)U_{n+1}(qa) + V_n(qa)V_{n+1}(qa)] \\
& -\left(1 - \frac{T_2^2}{T_1^2}\right) \frac{5T_1}{3T_0} \sum_{n=0}^{\infty} 2(n+1) \\
& \times [V_n(qa)U_{n+1}(qa) - U_n(qa)V_{n+1}(qa)] \\
& -\left(1 - \frac{T_2^2}{T_1^2}\right) \frac{3T_1}{2T_0(qa)^2} \sum_{n=0}^{\infty} 2n(n+1)(n+2) \\
& \times [V_n(qa)U_{n+1}(qa) - U_n(qa)V_{n+1}(qa)].
\end{aligned} \tag{14}$$

Combining the findings from the progressive and standing cases, we observe that $Y_{qst} = Y_p(1 - \frac{T_2^2}{T_1^2}) + Y_{st}(\frac{T_2 \sin(2qh)}{T_1})$. In this equation, Y_p represents the reduced SSRF under the plane progressive second sound. This expression serves as a link between the results obtained from the progressive and standing

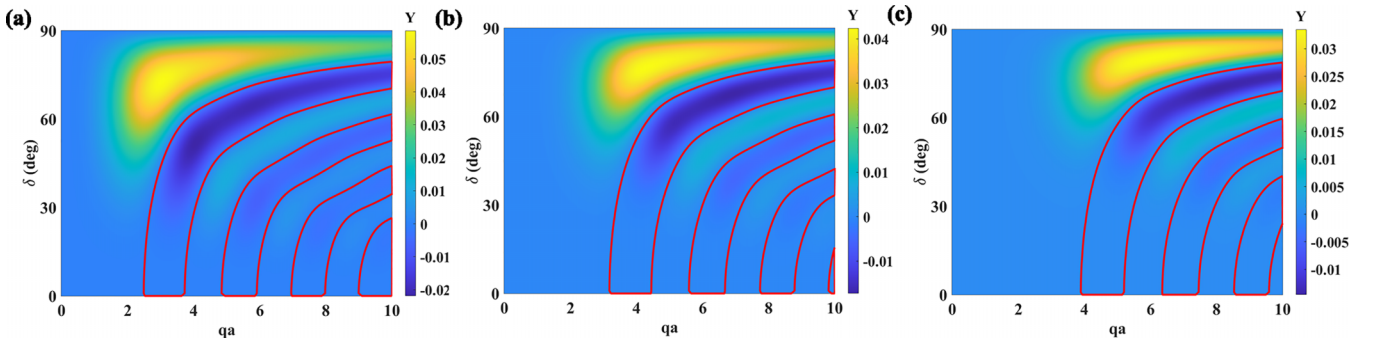


FIG. 3. Numerical results of the reduced second sound radiation force Y_{st} under the conditions of (a) second-order Bessel standing second sound as a function of qa and δ (unit: degree), (b) third-order Bessel standing second sound as a function of qa and δ , and (c) fourth-order Bessel standing second sound as a function of qa and δ , with $T_1/T_0 = 0.10$. The area enclosed by the red line is where $Y_{st} < 0$.

cases. Importantly, it is applicable not only to the plane case but also to the Bessel temperature field. The only difference is that $\sin(2qh)$ should be replaced by $\sin(2q_z h)$. We see when $T_1 = T_2$, the result coincides with the standing case, as the quasistanding temperature field reduces to a standing temperature field. Furthermore, if $T_1 = 0$, then Y_{st} is equivalent to the SSRF for progressive second sound.

IV. DISCUSSION AND CONCLUSION

In this paper, we have conducted a study on the SSRF (second sound radiation force) under the standing and quasistanding temperature field. In the case of a standing second sound field, the reduced SSRF can have both positive and negative values, even for the plane and zeroth-order Bessel standing temperature field. Similar results are found under high-order Bessel standing cases, as shown in Figs. 3(a)–3(c). However, it is important to note that the sign of Y_{st} indicates the direction relative to the temperature antinode or node, which is distinct from the progressive cases. We have also demonstrated that the results of the quasistanding temperature field can link the progressive case and standing case, which is of theoretical significance considering the existence of this relation even for high-order Bessel temperature field. In our research, we prioritize understanding the reduced radiation force, as we are particularly interested in the direction of this force. Through our calculations, we see that the magnitude of the second sound radiation force is approximately 10^{-9} N in a plane standing temperature field (see Fig. 4), as derived from Eq. (7). For simplicity, we have assumed $\sin(2qh) = 1$. We propose that one potential method to detect this force could be through the application of x-ray diffraction technique [51]. Given the elastic constant of the purity in crystals, the force can be determined by measuring the displacement of the purity particle from its equilibrium position.

Nevertheless, our focus in this paper remains on the hydrodynamic regime of thermal conduction force. For further studies, we could extend our analysis to other regimes, such as the diffusive and casir regimes [52–56]. Additionally, recent research has shown that density variation can induce a force effect for the fluid [57]. In the case of our solid-solid system, where we assume the background temperature is constant, we have neglected the corresponding density variation and have not considered the force effect. Our primary focus is on the interaction between second sound and impurity. Furthermore, we have assumed that the impurity is fixed, and there is a need for exploration regarding the force effect on movable impurities. Moreover, studying the force effect on nonadiabatic impurity particles proves to be an interesting research topic.

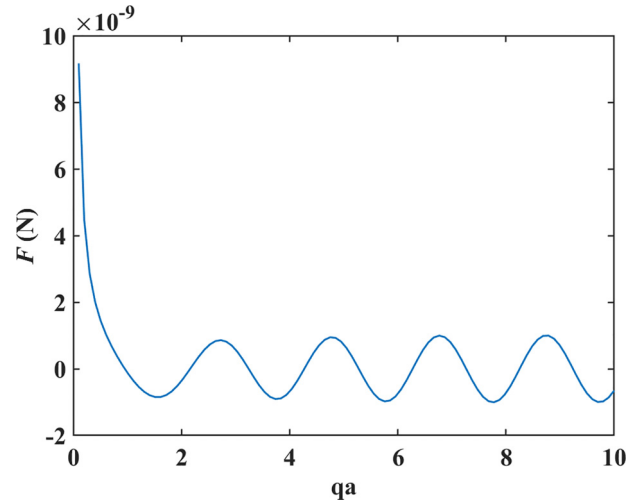


FIG. 4. Numerical results of the second sound radiation force F under the condition of plane standing second sound as a function of qa with $T_1/T_0 = 0.10$.

While our investigation is primarily centered on the interaction between second sound and a spherical particle within this study, corresponding to the force exerted on a purity particle in crystals by the temperature field, it is theoretically feasible to explore the force effect between the second sound and a cylinder as well [58].

In summary, building upon the research on second sound radiation force for progressive second sound, we have extended our analysis to incorporate the standing and quasistanding cases. We have revealed distinct characteristics of the second radiation force for these cases. Additionally, we have explored the relationship between the progressive, standing, and quasistanding cases. This not only enriches the fundamental theory of second sound radiation force but also paves the way for future studies in more complex scenarios [59]. In terms of applications, our study offers people an additional degree of freedom to manipulate the local thermal conductivity of dielectric crystals.

ACKNOWLEDGMENTS

We would like to express our gratitude to Dr. LiuJun Xu of the Graduate School of China Academy of Engineering Physics for his valuable and insightful suggestions that have helped us improve our research work. We gratefully acknowledge funding from the National Natural Science Foundation of China (Grants No. 12035004 and No. 12320101004) and the Innovation Program of Shanghai Municipal Education Commission (Grant No. 2023ZKZD06).

- [1] X. Zhou, X. Xu, and J. Huang, Adaptive multi-temperature control for transport and storage containers enabled by phase-change materials, *Nat. Commun.* **14**, 5449 (2023).
 [2] L. Xu, J. Liu, G. Xu, J. Huang, and C.-W. Qiu, Giant, magnet-free, and room-temperature hall-like heat transfer, *Proc. Natl. Acad. Sci. USA* **120**, e2305755120 (2023).

- [3] F. Yang, Z. Zhang, L. Xu, Z. Liu, P. Jin, P. Zhuang, M. Lei, J. Liu, J.-H. Jiang, X. Ouyang *et al.*, Controlling mass and energy diffusion with metamaterials, *Rev. Mod. Phys.* **96**, 015002 (2024).
 [4] L. Xu, G. Xu, J. Huang, and C.-W. Qiu, Diffusive Fizeau drag in spatiotemporal thermal metamaterials, *Phys. Rev. Lett.* **128**, 145901 (2022).

- [5] L. Xu, G. Xu, J. Li, Y. Li, J. Huang, and C.-W. Qiu, Thermal Willis coupling in spatiotemporal diffusive metamaterials, *Phys. Rev. Lett.* **129**, 155901 (2022).
- [6] P. Jin, J. Liu, L. Xu, J. Wang, X. Ouyang, J.-H. Jiang, and J. Huang, Tunable liquid–solid hybrid thermal metamaterials with a topology transition, *Proc. Natl. Acad. Sci. USA* **120**, e2217068120 (2023).
- [7] Z. Zhang, L. Xu, T. Qu, M. Lei, Z.-K. Lin, X. Ouyang, J.-H. Jiang, and J. Huang, Diffusion metamaterials, *Nat. Rev. Phys.* **5**, 218 (2023).
- [8] Y. Li, W. Li, T. Han, X. Zheng, J. Li, B. Li, S. Fan, and C.-W. Qiu, Transforming heat transfer with thermal metamaterials and devices, *Nat. Rev. Mater.* **6**, 488 (2021).
- [9] P. L. Palla, G. Patera, F. Cleri, and S. Giordano, A stochastic force model for the ballistic–diffusive transition of heat conduction, *Phys. Scr.* **95**, 075703 (2020).
- [10] S. Lepri, R. Livi, and A. Politi, Thermal conduction in classical low-dimensional lattices, *Phys. Rep.* **377**, 1 (2003).
- [11] A. Dhar, Heat transport in low-dimensional systems, *Adv. Phys.* **57**, 457 (2008).
- [12] P. Jin, L. Xu, G. Xu, J. Li, C.-W. Qiu, and J. Huang, Deep learning-assisted active metamaterials with heat-enhanced thermal transport, *Adv. Mater.* **36**, 2305791 (2024).
- [13] F. Gaeta, Radiation pressure theory of thermal diffusion in liquids, *Phys. Rev.* **182**, 289 (1969).
- [14] F. S. Gaeta, E. Ascolese, and B. Tomicki, Radiation forces associated with heat propagation in nonisothermal systems, *Phys. Rev. A* **44**, 5003 (1991).
- [15] C. Albanese, P. Dell’Aversana, and F. S. Gaeta, Experimental detection of forces produced by the flow of heat, *Phys. Rev. Lett.* **79**, 4151 (1997).
- [16] H. Tan, Y. Qiu, L. Xu, and J. Huang, Tunable thermal conduction force without macroscopic temperature gradients, *Phys. Rev. E* **108**, 034105 (2023).
- [17] S. Huberman, R. A. Duncan, K. Chen, B. Song, V. Chiloyan, Z. Ding, A. A. Maznev, G. Chen, and K. A. Nelson, Observation of second sound in graphite at temperatures above 100 K, *Science* **364**, 375 (2019).
- [18] Z. Ding, K. Chen, B. Song, J. Shin, A. A. Maznev, K. A. Nelson, and G. Chen, Observation of second sound in graphite over 200 K, *Nat. Commun.* **13**, 285 (2022).
- [19] A. Beardo, M. López-Suárez, L. A. Pérez, L. Sendra, M. I. Alonso, C. Melis, J. Bafaluy, J. Camacho, L. Colombo, R. Rurali *et al.*, Observation of second sound in a rapidly varying temperature field in Ge, *Sci. Adv.* **7**, eabg4677 (2021).
- [20] H. E. Jackson, C. T. Walker, and T. F. McNelly, Second sound in NaF, *Phys. Rev. Lett.* **25**, 26 (1970).
- [21] V. Narayanamurti and R. Dynes, Observation of second sound in bismuth, *Phys. Rev. Lett.* **28**, 1461 (1972).
- [22] D. Osborne, Second sound in liquid helium II, *Proc. Phys. Soc. A* **64**, 114 (1951).
- [23] J. Callaway, Model for lattice thermal conductivity at low temperatures, *Phys. Rev.* **113**, 1046 (1959).
- [24] R. Guyer and J. Krumhansl, Thermal conductivity, second sound, and phonon hydrodynamic phenomena in nonmetallic crystals, *Phys. Rev.* **148**, 778 (1966).
- [25] J. Ward and J. Wilks, The velocity of second sound in liquid helium near the absolute zero, *Lond. Edinb. Dublin Philos. Mag. J. Sci.* **42**, 314 (1951).
- [26] R. B. Dingle, Derivation of the velocity of second sound from Maxwell’s equation of transfer, *Proc. Phys. Soc. A* **65**, 374 (1952).
- [27] P. C. Kwok, Dispersion and damping of second sound in non-isotropic solids, *Phys. Phys. Fiz.* **3**, 221 (1967).
- [28] J. A. Sussmann and A. Thellung, Thermal conductivity of perfect dielectric crystals in the absence of umklapp processes, *Proc. Phys. Soc.* **81**, 1122 (1963).
- [29] H. Beck, P. Meier, and A. Thellung, Phonon hydrodynamics in solids, *Physica Status Solidi (a)* **24**, 11 (1974).
- [30] M. Chester, Second sound in solids, *Phys. Rev.* **131**, 2013 (1963).
- [31] E. W. Prohofsky and J. A. Krumhansl, Second-sound propagation in dielectric solids, *Phys. Rev.* **133**, A1403 (1964).
- [32] X. Li, X. Luo, S. Wang, K. Xie, X.-P. Liu, H. Hu, Y.-A. Chen, X.-C. Yao, and J.-W. Pan, Second sound attenuation near quantum criticality, *Science* **375**, 528 (2022).
- [33] M. Baudoin and J.-L. Thomas, Acoustic tweezers for particle and fluid micromanipulation, *Annu. Rev. Fluid Mech.* **52**, 205 (2020).
- [34] O. A. Sapozhnikov and M. R. Bailey, Radiation force of an arbitrary acoustic beam on an elastic sphere in a fluid, *J. Acoust. Soc. Am.* **133**, 661 (2013).
- [35] Z. Gong and M. Baudoin, Acoustic radiation torque on a particle in a fluid: An angular spectrum based compact expression, *J. Acoust. Soc. Am.* **148**, 3131 (2020).
- [36] G. T. Silva, An expression for the radiation force exerted by an acoustic beam with arbitrary wavefront (L), *J. Acoust. Soc. Am.* **130**, 3541 (2011).
- [37] D. Baresch, J.-L. Thomas, and R. Marchiano, Three-dimensional acoustic radiation force on an arbitrarily located elastic sphere, *J. Acoust. Soc. Am.* **133**, 25 (2013).
- [38] G. Silva, T. Lobo, and F. Mitri, Radiation torque produced by an arbitrary acoustic wave, *Europhys. Lett.* **97**, 54003 (2012).
- [39] Z. Gong, P. L. Marston, and W. Li, Reversals of acoustic radiation torque in Bessel beams using theoretical and numerical implementations in three dimensions, *Phys. Rev. Appl.* **11**, 064022 (2019).
- [40] Z. Gong and M. Baudoin, Equivalence between angular spectrum-based and multipole expansion-based formulas of the acoustic radiation force and torque, *J. Acoust. Soc. Am.* **149**, 3469 (2021).
- [41] P. L. Marston, Axial radiation force of a Bessel beam on a sphere and direction reversal of the force, *J. Acoust. Soc. Am.* **120**, 3518 (2006).
- [42] P. L. Marston, Negative axial radiation forces on solid spheres and shells in a Bessel beam, *J. Acoust. Soc. Am.* **122**, 3162 (2007).
- [43] F. G. Mitri, Langevin acoustic radiation force of a high-order Bessel beam on a rigid sphere, *IEEE Trans. Ultrason. Ferroelectr. Freq. Control* **56**, 1059 (2009).
- [44] P. L. Marston, Radiation force of a helicoidal Bessel beam on a sphere, *J. Acoust. Soc. Am.* **125**, 3539 (2009).
- [45] L. Zhang and P. L. Marston, Geometrical interpretation of negative radiation forces of acoustical Bessel beams on spheres, *Phys. Rev. E* **84**, 035601(R) (2011).
- [46] M. Gong, Y. Qiao, Z. Fei, Y. Li, J. Liu, Y. Mao, A. He, and X. Liu, Non-diffractive acoustic beams produce negative radiation force in certain regions, *AIP Adv.* **11**, 065029 (2021).

- [47] X.-D. Fan and L. Zhang, Phase shift approach for engineering desired radiation force: acoustic pulling force example, *J. Acoust. Soc. Am.* **150**, 102 (2021).
- [48] T. Hasegawa, Acoustic radiation force on a sphere in a quasi-stationary wave field-theory, *J. Acoust. Soc. Am.* **65**, 32 (1979).
- [49] F. Mitri, Acoustic radiation force on a sphere in standing and quasi-standing zero-order Bessel beam tweezers, *Ann. Phys.* **323**, 1604 (2008).
- [50] F. Mitri, Acoustic radiation force of high-order Bessel beam standing wave tweezers on a rigid sphere, *Ultrasonics* **49**, 794 (2009).
- [51] C. L. Williams, C. Kale, S. A. Turnage, L. S. Shannahan, B. Li, K. N. Solanki, R. Becker, T. C. Hufnagel, and K. T. Ramesh, Real-time observation of twinning-detwinning in shock-compressed magnesium via time-resolved *in situ* synchrotron XRD experiments, *Phys. Rev. Mater.* **4**, 083603 (2020).
- [52] R. S. Sorbello, Phonon-radiation force in defect crystal lattices, *Phys. Rev. B* **6**, 4757 (1972).
- [53] M. Gerl, Calculation of the force acting on an impurity in a metal submitted to an electric field or a temperature gradient, *Z. Naturforsch. A* **26**, 1 (1971).
- [54] L.-J. Xu and J.-P. Huang, Active thermal wave cloak, *Chin. Phys. Lett.* **37**, 120501 (2020).
- [55] P. Jin, L. Xu, T. Jiang, L. Zhang, and J. Huang, Making thermal sensors accurate and invisible with an anisotropic monolayer scheme, *Int. J. Heat Mass Transf.* **163**, 120437 (2020).
- [56] P. Zhuang and J. Huang, Multiple control of thermoelectric dual-function metamaterials, *Int. J. Mech. Syst. Dyn.* **3**, 127 (2023).
- [57] J. T. Karlsen, P. Augustsson, and H. Bruus, Acoustic force density acting on inhomogeneous fluids in acoustic fields, *Phys. Rev. Lett.* **117**, 114504 (2016).
- [58] D. Haydock, Calculation of the radiation force on a cylinder in a standing wave acoustic field, *J. Phys. A: Math. Gen.* **38**, 3279 (2005).
- [59] C.-X. Zhang, T.-J. Li, L.-J. Xu, and J.-P. Huang, Dust-induced regulation of thermal radiation in water droplets, *Chin. Phys. Lett.* **40**, 054401 (2023).